Asian Journal of Chemistry; Vol. 29, No. 7 (2017), 1466-1470

ASIAN JOURNAL OF CHEMISTRY

https://doi.org/10.14233/ajchem.2017.20525

Physico-Chemical Properties of $LiM_{0.10}Mn_{1.90}O_4$ (M: Co, Ni, Cr) for Potential Cathode Materials

DYAH PURWANINGSIH[1,2,*], ROTO ROTO[1], HARI SUTRISNO[2] and AGUS PURWANTO[3]

[1]Department of Chemistry, Faculty of Mathematics and Natural Sciences, Gadjah Mada University, Yogyakarta, Indonesia
[2]Department of Chemistry Education, Faculty of Mathematics and Natural Sciences, Yogyakarta State University, Yogyakarta, Indonesia
[3]Department of Chemical Engineering, Faculty of Engineering, Universitas Sebelas Maret, Surakarta, Indonesia

*Corresponding author: Tel: +62 81 327563208; E-mail: dyah_purwaningsih@uny.ac.id

Received: 19 January 2017; *Accepted*: 9 March 2017; *Published online*: 13 May 2017; AJC-18375

Transition metal-doped spinel cathode materials of $LiM_{0.1}Mn_{1.9}O_4$ (M: Co, Ni, Cr) were prepared by solid-state reaction. The structure and morphology of the products were investigated by X-ray photoelectron spectroscopy, X-ray diffraction, Rietveld refinement and SEM-EDX. The oxidation states of Mn, Co, Ni and Cr were found to be 3+/4+, 2+, 2+ and 3+, respectively as revealed by X-ray photoelectron spectroscopy. SEM-EDX shows uniform particles and the particle size was about 200-700 nm ranges. The diffraction peaks of the prepared solids corresponded to a single phase of cubic spinel structure with a space group Fd3m. Doping of Co, Ni and Cr causes lattice parameters to decrease. The prepared materials have ionic conductivity where $LiCo_{0.10}Mn_{1.90}O_4$ has the highest capacitance.

Keywords: Physico-chemical properties, $LiM_{0.10}Mn_{1.90}O_4$, Potential cathode.

INTRODUCTION

The development of cathodes for lithium-ion battery has received considerable attention in recent years. Among others, lithium ion battery is used extensively as rechargeable battery [1,2]. For cathode materials studied, $LiMn_2O_4$ spinel was considered as a good cathode due to the higher capacity, cycleability and environmentally friendly [3,4]. However, $LiMn_2O_4$ electrodes suffers from rapid capacity fade redox during cycling [5,6]. To minimize the capacity fade, replacing Mn^{3+} ions by other transition metal ions such as Co, Ni and Cr is one way [7,8]. The presence of cobalt in the structure can improve the capacity retention during cycling by stabilizing the structure [9]. Doping nickel can reduce the lattice parameters and electrical conductivity and increase the capacity of $LiMn_2O_4$ [10,11]. Adding chromium can reduce the $LiMn_2O_4$ lithium ion composition, stabilize the single phase spinel structure and increase retention capacity upon charging and discharging [12,13].

Many researchers have conducted syntheses of $LiMn_2O_4$ with various methods. The synthesis is usually conducted at high temperature to maintain the stability of the spinel phase. Sol-gel, condensing gas and spray pyrolysis methods are believed to retain the phase [14-16]. Problems faced in the synthesis are high cost and not feasable since it was done at high temperature [17,18]. In the present study, we have prepared transition metal-doped $LiM_{0.1}Mn_{1.9}O_4$ (M: Co, Ni, Cr) positive electrodes through reflux and solid-state reaction. We mainly focus on analysis of physico-chemical properties of $LiM_{0.1}Mn_{1.9}O_4$ cathodes by X-ray photoelectron microscopic measurement, X-ray diffraction, SEM-EDX and AC impedance measurement.

EXPERIMENTAL

Synthesis of MnO_2 and $LiM_xMn_{2-x}O_4$: An analytical grade of $Mn(CH_3COO)_2$ and $Na_2S_2O_8$ (Aldrich) were used to prepare MnO_2 nanorods by reflux technique. All other chemicals were used without as they were received. In a typical synthesis, $Mn(CH_3COO)_2$ and $Na_2S_2O_8$ were dissolved at room temperature with a molar ratio of 1:1 in 80 mL deionized distilled water by magnetic stirring to form a clear homogeneous solution. The mixed solution was transferred into boiling flask and heated at 120 °C for 12 h. The obtained powder was subsequently dried at 110 °C for 12 h in air [19].

A typical synthesis of $LiM_{0.10}M_{1.90}O_4$ is as the following. 1 mole of LiOH, 0.10 moles of $Co(CH_3COO)_2$ and 1.90 mol of as-synthesized MnO_2 were dispersed into high purity ethanol to form a thick slurry, stirred to form fine mixture for several hours and dried at room temperature. The above process was repeated two to three times to produce a well-mixed powder. The $LiMn_2O_4$ powder was then ignited at 750 °C for 10 h. The same procedure was used for synthesis $LiMn_{0.10}Mn_{1.90}O_4$, $LiNi_{0.10}Mn_{1.90}O_4$ and $LiCr_{0.10}Mn_{1.90}O_4$ [20,21].

Characterization of $LiM_{0.10}Mn_{1.90}O_4$ microstructure: The cathode material underwent X-ray photoelectron

spectroscopy (XPS) analysis to calculate the valence states of manganese and the substituted transition metal ions using Thermo VG Scientific instrument, Multilab 2000. The morphologies were characterized using JEOL JSM-6510LA scanning electron microscopes (SEM). The influence of the metal load on the structural characteristics of M doped $LiMn_2O_4$ was studied using energy dispersive X-ray spectroscopy (EDX), which also used to analyze the presence of M, O and Mn elements in the prepared materials. The produced MnO_2 and $LiM_{0.10}Mn_{1.90}O_4$ were examined using powder X-ray diffractometer. The XRD patterns were obtained on Rigaku Miniflex 600-Benchtop XRD instrument, operated in the Bragg configuration using CuK_α radiation ($\lambda = 1.5406$ Å) at ambient temperature. The instrument was set to operate at 40 kV and 15 mA. The measurement was recorded in steps of 0.02° with a count time of 15 s/step. The intensities were determined in the 2θ interval ranging from 20° to 90°. To refine each spectrum, the direct method was carried out by using the Fullprof software by Roisnel and Rodriguez Carvajal in WinPLOTR package program and diamond. The following parameters were refined: unit cell, scale factor and full width at half-maximum (FWHM). The electrical measurement was tested by using LCR-8105G GW Instek 20 Hz-5 MHz. Samples were pressed into pellets 6.705 mm and then sintered in the air between 1223 and 1373 K for 24 h. Blocking electrodes were deposited on both sides of the pellet by conductive silver paint. The resistance value is obtained by fitting Z *vs.* Z".

RESULTS AND DISCUSSION

X-Ray photoelectron spectroscopy: Identification of the metals' oxidation states in $LiM_{0.10}Mn_{1.90}O_4$ (M: Mn, Co, Ni, Cr) was performed using AlK_α X-ray source. The binding energy was recorded from 0 to 1200 eV. It showed that Li, Mn, M and O are present in the sample. According to the spectra, the presence of Li in the powders was observed clearly at 55.08 eV for $LiMn_2O_4$. The Mn 2p ($2p^{3/2}$ and $2p^{1/2}$) doublet peaks were observed for native $LiMn_2O_4$. The peaks at 641.98 and 643.28 eV can be attributed to Mn $2p^{3/2}$ and Mn $2p^{1/2}$. The previous reports [22] showed that the XPS binding energy for Mn^{3+} and Mn^{4+} ions at 641.9 and 643.2 eV, to indicate the presence of mixed oxidation state of Mn in the structure. The XPS measurement was also performed for the rest of the doping products. According to the reference, the peak center for Co $2p^3$, Ni $2p^3$ and Cr $2p^3$ were positioned at 779.07, 854.88 and 576.58 eV, respectively (Fig. 1). We can confirmed the oxidation of metals from the observed binding energy.

SEM-EDX: The morphology of the prepared powders has been observed by scanning electron microscopy and the

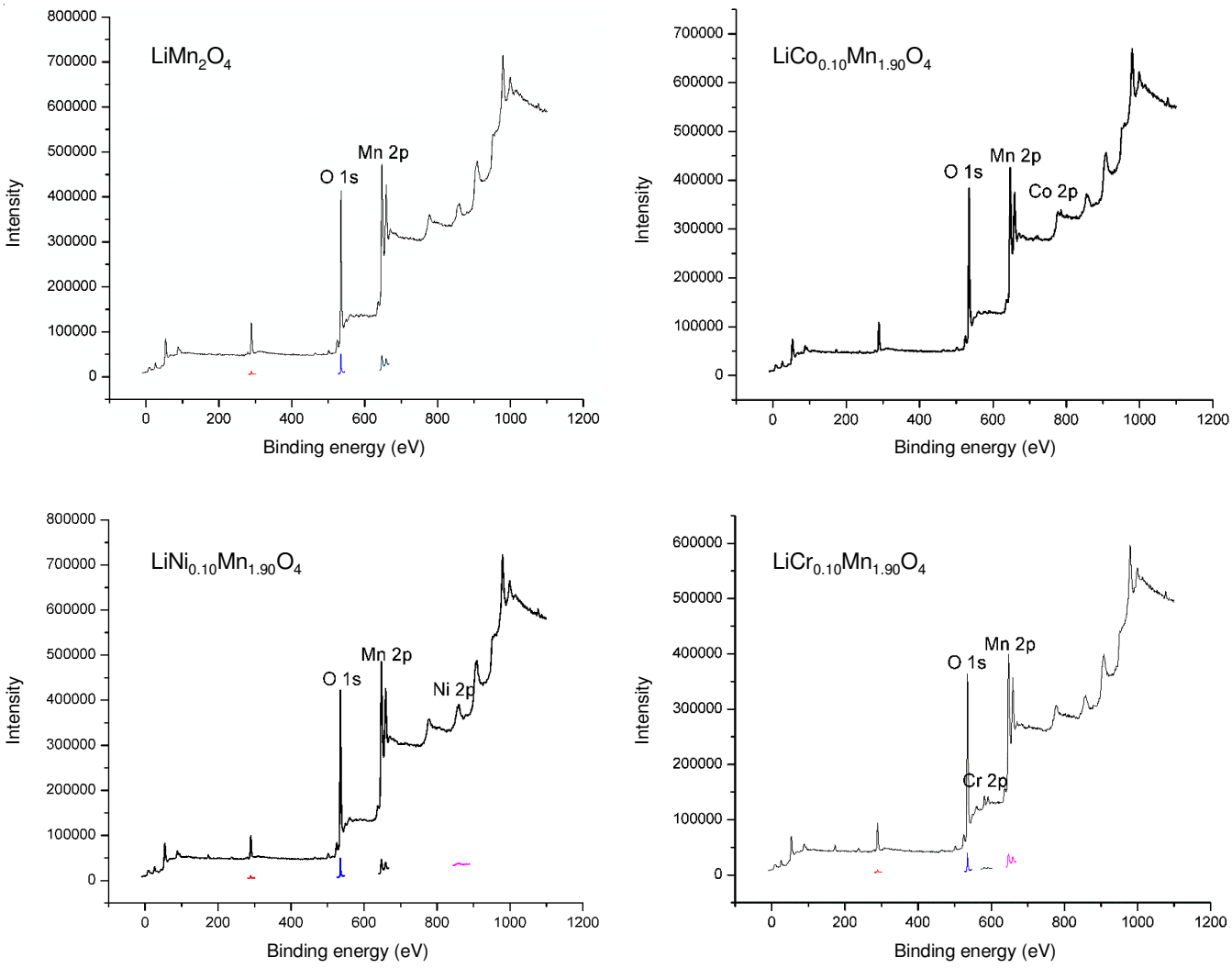

Fig. 1. XPS scan spectra of $LiM_{0.10}Mn_{1.90}O_4$ (M: Mn, Co, Ni, Cr)

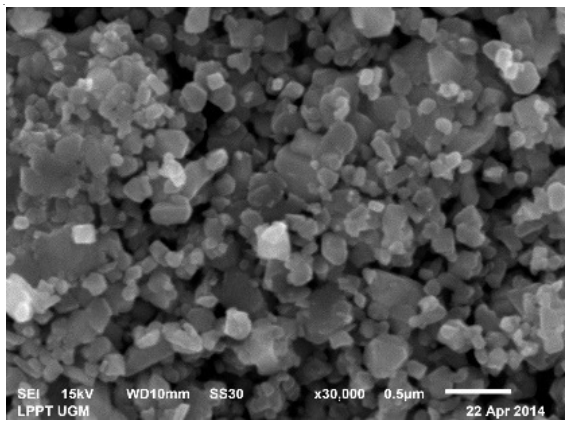

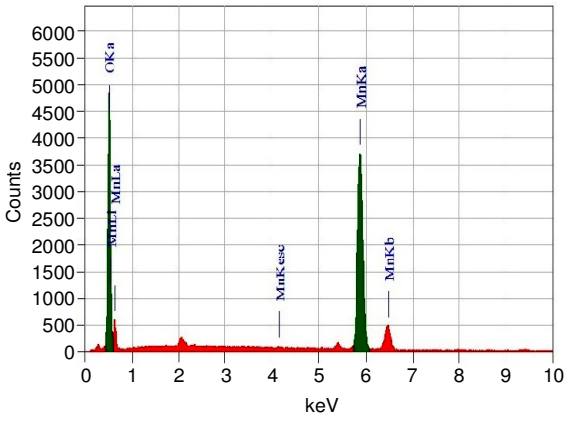

$LiMn_2O_4$

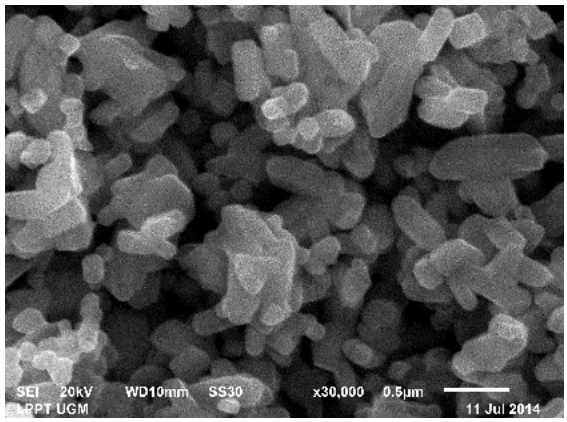

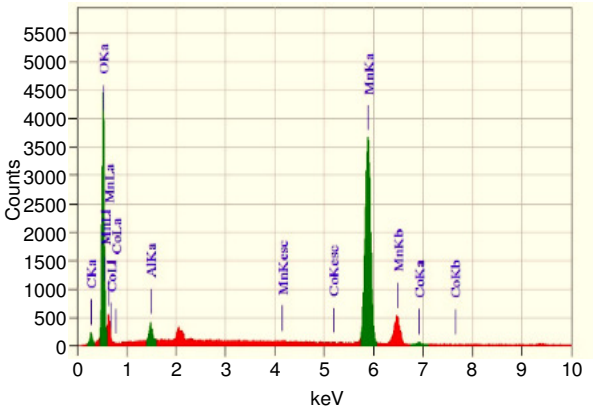

$LiCo_{0.10}Mn_{1.90}O_4$

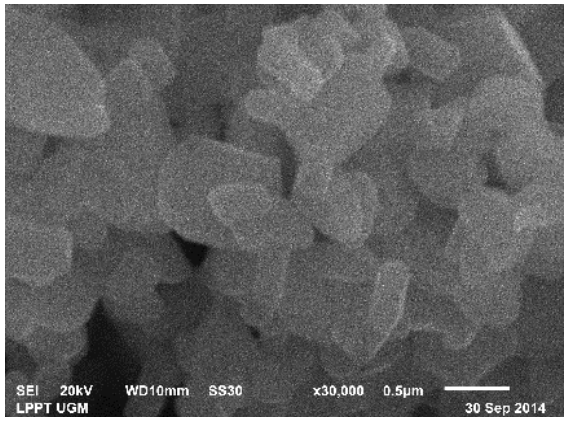

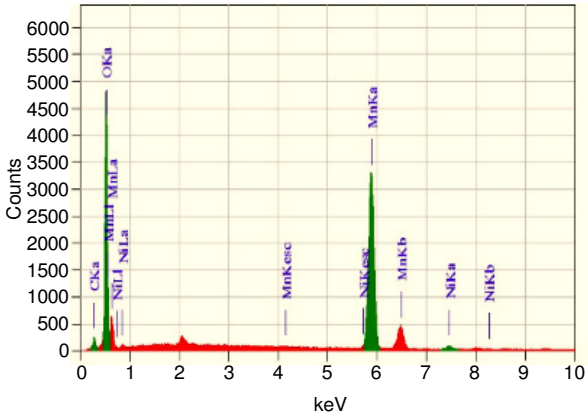

$LiNi_{0.10}Mn_{1.90}O_4$

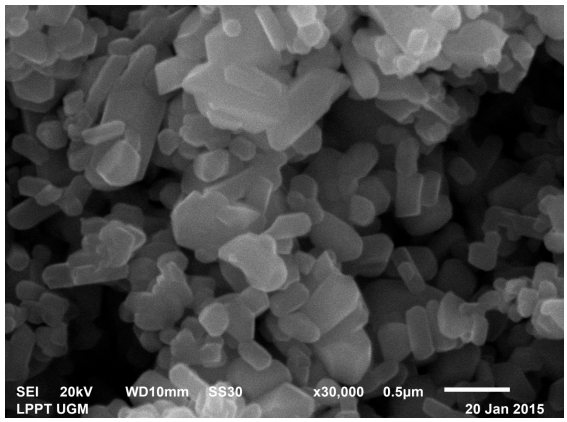

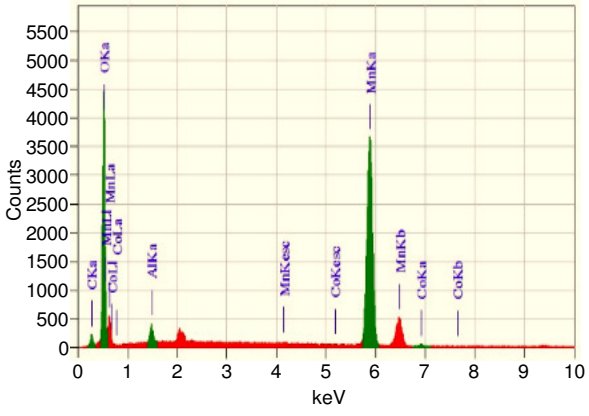

$LiCr_{0.10}Mn_{1.90}O_4$

Fig. 2. SEM-EDX of $LiM_{0.10}Mn_{1.90}O_4$ (M: Mn, Co, Ni, Cr)

micrographs are shown in Fig. 2. It can be seen from the figure that the average particle size in $LiMn_2O_4$ is smaller than the $LiM_{0.10}Mn_{1.90}O_4$ (M: Co, Ni, Cr). The particle has uniform particle distribution from 200-700 nm. It is observed that average particle size for $LiMn_2O_4$, $LiCo_{0.10}Mn_{1.90}O_4$, $LiNi_{0.10}Mn_{1.90}O_4$ and $LiCr_{0.10}Mn_{1.90}O_4$ are among 135; 150-250; 570 and 178 nm, respectively. This might be explained on the basis of the fact that in this case, the drive for the nucleation of Mn has overcome the drive of the growth of the particles. It is clear that nano size particle is good for battery performance [23]. The shape of the particle nearly spherical and octahedron-type. The particles in slightly agglomerated state are also observed and could be beneficial towards achieving good packing density of the material compared to higher bulk capacity. From the EDS, it is also clearly observed that the stoichiometry of Mn; M and O are well-fitted to $LiM_{0.10}Mn_{1.90}O_4$ (M: Co, Ni, Cr).

X-Ray diffraction: Fig. 3 shows the XRD patterns of $LiM_{0.10}Mn_{1.90}O_4$ (M: Mn, Co, Ni, Cr). Its diffraction peaks were perfectly indexed to a pure cubic spinel phase. No clear difference was observed among the XRD patterns of $LiMn_2O_4$, $LiCo_{0.10}Mn_{1.90}O_4$, $LiNi_{0.10}Mn_{1.90}O_4$ and $LiCr_{0.10}Mn_{1.90}O_4$. The broad diffraction peaks of the powders indicated that the particle size was small. Peak broadening in nanoparticles can originate from variation in lattice spacings, caused by lattice strain as the size decreases and the crystallite were estimated among 36-42 nm using Scherrer equation [24]. Analysis using winPlotr package program and diamond shows that all products were identified as a single-phase cubic with a space group of Fd3m where lithium ions occupy the tetrahedral (8a) sites. Meanwhile, Mn^{3+} and Mn^{4+} and M^{2+}/M^{3+} ions are located at the octahedral centers (16d) and O^{2-} ions are located at the edge (32e). The sharp (400) peak in the XRD patterns of all the compounds reveals that high-crystallized manganese oxides were synthesized.

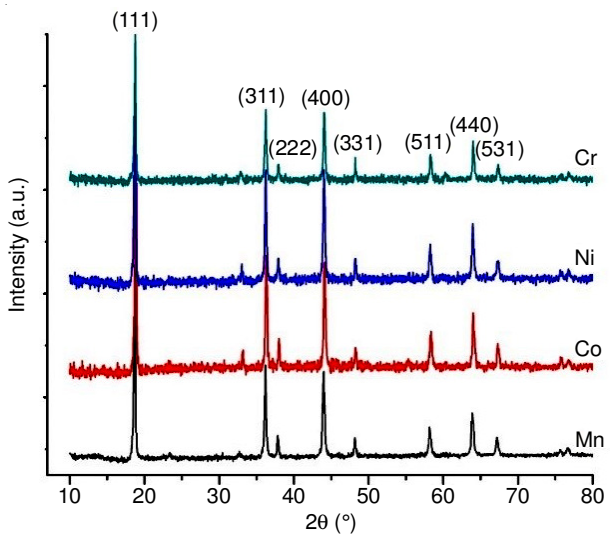

Fig. 3. X-ray powder diffraction patterns of $LiM_{0.10}Mn_{1.90}O_4$ (M: Mn, Co, Ni, Cr) prepared by solid-state reaction

Table-1 shows the lattice parameters and space group of the refined structure of the materials. It shows that lattice parameters are observed to decrease with the doping of M in the prepared $LiM_{0.10}Mn_{1.90}O_4$. This is believed to be due to partial substitution of Mn^{3+} ions by M^{3+} or M^{2+} [21]. A slightly reduced in Mn^{3+} content and higher in Mn^{4+} content appeared in all $LiM_{0.10}Mn_{1.90}O_4$ powders. These trends are expected to suppress Jahn-Teller distortion for $Li/LiM_{0.10}Mn_{1.90}O_4$ cells during a series of charge and discharge when it is used in the battery [25]. The rationale for this phenomenon can be speculated as (1) the radius for Mn^{3+} ions (0.645 Å) is larger than that of Mn^{4+} ions (0.53 Å) and (2) the M/Mn-O interatomic distance increases with doping of M. It is apparently to contribute to the lattice contraction of $LiM_{0.10}Mn_{1.90}O_4$ in line with the decrease of the volume cells (Fig. 4). It helps to stabilize spinel crystal structure during the electrochemical cycling and improve its electro-chemical properties [26].

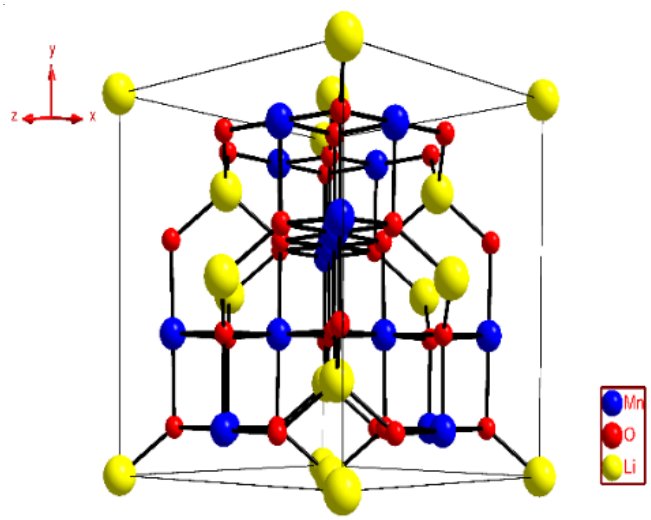

Fig. 4. Microstructure of $LiM_{0.10}Mn_{1.90}O_4$ (M: Co, Ni, Cr)

Electrical conductivity: The curve Z *vs.* Z" in Fig. 5 shows that the highest impedance is $LiMn_2O_4$ compared to the other transition metals. It indicates that the highest conductivity was $LiCo_{0.10}Mn_{1.90}O_4$. Table-2 shows that $LiCo_{0.10}Mn_{1.90}O_4$ has the highest capacitance compared to the other solids. Based on the range of conductivity [27], we can classify the conductivity into ionic conductivity and electronic conductivity. Ionic conductivity consists of grain conductivity and grain-

TABLE-1
LATTICE PARAMETERS, SPACE GROUP AND Li-O/M/Mn-O DISTANCE OF THE $LiM_{0.10}Mn_{1.90}O_4$ (M: Mn, Co, Ni, Cr) SAMPLES PREPARED BY SOLID-STATE REACTIONS

Samples	Lattice parameter (Å) a = b = c	Space group	Li-O (Å)	Mn/M-O (Å)	Agreement factor from direct method		
					R_1	wR_2	GooF
$LiMn_2O_4$	8.2452	Fd3m	1.854	2.032	0.0917	0.1640	3.518
$LiCo_{0.10}Mn_{1.90}O_4$	8.2313	Fd3m	1.771	2.064	0.0955	0.2532	2.101
$LiNi_{0.10}Mn_{1.90}O_4$	8.2371	Fd3m	1.778	2.059	0.1022	0.2919	3.993
$LiCr_{0.10}Mn_{1.90}O_4$	8.2333	Fd3m	1.762	2.071	0.0821	0.2526	2.272

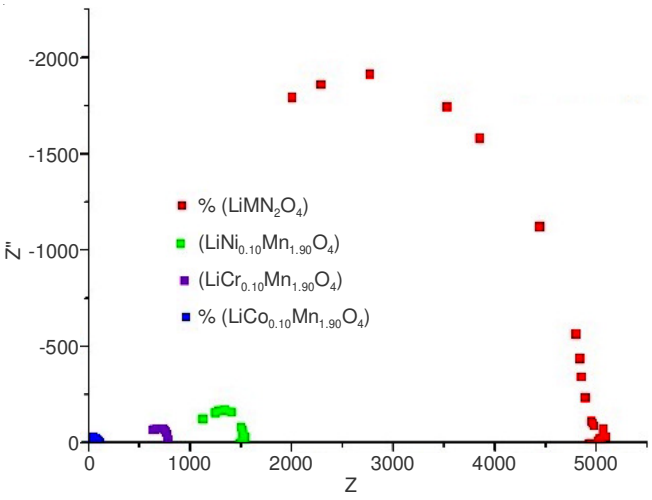

Fig. 5. Curve Z *vs*. Z" of $LiM_{0.10}Mn_{1.90}O_4$ (M: Mn, Co, Ni, Cr)

TABLE-2
CAPACITANCE AND CONDUCTIVITY
$LiM_{0.10}Mn_{1.90}O_4$ (M: Co, Ni, Cr)

Materials	Capacitance (F)	Conductivity (S/cm)
$LiMn_2O_4$	2.87×10^{-11}	0.000156
$LiCo_{0.10}Mn_{1.90}O_4$	9.72×10^{-9}	0.005692
$LiNi_{0.10}Mn_{1.90}O_4$	2.61×10^{-9}	0.001632
$LiCr_{0.10}Mn_{1.90}O_4$	2.40×10^{-9}	0.004277

boundary conductivity. From the calculation, it is observed that the conductivity obtained in $LiM_{0.10}Mn_{1.90}O_4$ (M: Co, Ni, Cr) were ionic conductivity. It could be beneficial for battery technology and is expected to give a better performance.

Conclusion

The $LiM_{0.10}Mn_{1.90}O_4$ (M: Co, Ni, Cr) have been prepared by solid-state reaction. The XPS results revealed metals such as Mn, Ni, Co and Cr in $LiM_{0.10}Mn_{1.90}O_4$ exist in the 3+, 2+, 2+ and 3+ oxidation states, respectively. Results of the SEM-EDX data show that the prepared compounds have particle sizes in the range 200-700 nm. The diffraction peaks of all the samples correspond to a single phase of cubic spinel structure with a space group Fd3m. Therefore, the standard spinel structure was maintained by doping with other ions, which occupy 16d octahedral sites. Doping of Co, Ni and Cr tends to decrease the lattice parameters compared to the pure $LiMn_2O_4$. The conductivity adopting of ionic conductivity and the highest capacitance was $LiCo_{0.10}Mn_{1.90}O_4$. It could be beneficial in the battery technology and is expected to give a better performance.

ACKNOWLEDGEMENTS

The authors thank the Ministry of Research, Technology and Higher Education for financial support through the Doctoral Dissertation Program. We are grateful to Dr. Liu Yan of Institute of Chemical and Engineering Sciences Singapore and Dr. Is Fatimah of the The Islamic University of Indonesia for analysis with X-ray Photoelectron Spectroscopy. We would also like to thank Dr. Dani Bustaman of National Nuclear Energy Agency of Indonesia for LCR-meter use.

REFERENCES

1. K.E. Aifantis, S.A. Hackney and R.V. Kumar, High Energy Density Lithium Batteries, Wiley-VCH Verlag GmbH & Co. KGaA, Weinheim, Germany (2010).
2. M. Hu, X. Pang and Z. Zhou, *J. Power Sources*, **237**, 229 (2013); https://doi.org/10.1016/j.jpowsour.2013.03.024.
3. J.W. Fergus, *J. Power Sources*, **195**, 939 (2010); https://doi.org/10.1016/j.jpowsour.2009.08.089.
4. J. Chen, *Materials*, **6**, 156 (2013); https://doi.org/10.3390/ma6010156.
5. J. Vetter, P. Novak, M.R. Wagner, C. Veit, K.C. Möller, J.O. Besenhard, M. Winter, M. Wohlfahrt-Mehrens, C. Vogler and A. Hammouche, *J. Power Sources*, **147**, 269 (2005); https://doi.org/10.1016/j.jpowsour.2005.01.006.
6. J.-T. Hwang, S.-B. Park, C.-K. Park and H. Jang, *Bull. Korean Chem. Soc.*, **32**, 3952 (2011); https://doi.org/10.5012/bkcs.2011.32.11.3952.
7. Q. Liu, S. Wang, H. Tan, Z. Yang and J. Zeng, *Energies*, **6**, 1718 (2013); https://doi.org/10.3390/en6031718.
8. J. Yan, H. Liu, Y. Wang, X. Zhao, Y. Mi and B. Xia, *Ionics*, **21**, 1835 (2015); https://doi.org/10.1007/s11581-015-1371-9.
9. Y.-P. Fu, C.-H. Lin, Y.-H. Su, J.-H. Jean and S.-H. Wu, *Ceram. Int.*, **30**, 1953 (2004); https://doi.org/10.1016/j.ceramint.2003.12.183.
10. X. Gu, X. Li, L. Xu and H. Xu, *Int. J. Electrochem. Sci.*, **7**, 2504 (2012).
11. H.L. Wang, Ph.D. Thesis, 4d Transition Metal Doped $LiNi_{0.5}Mn_{1.5}O_4$ for High Power Lithium Batteries, Department of Mechanical Engineering, National University of Singapore, Singapore (2011).
12. M. Aklalouch, J.M. Amarilla, R.M. Rojas, I. Saadoune and J.M. Rojo, *J. Power Sources*, **185**, 501 (2008); https://doi.org/10.1016/j.jpowsour.2008.06.074.
13. G.M. Song, Y.J. Wang and Y. Zhou, *J. Power Sources*, **128**, 270 (2004); https://doi.org/10.1016/j.jpowsour.2003.10.002.
14. V.G. Kumar, J.S. Gnanaraj, S. Ben-David, D.M. Pickup, E.R.H. van-Eck, A. Gedanken and D. Aurbach, *Chem. Mater.*, **15**, 4211 (2003); https://doi.org/10.1021/cm030104j.
15. Y.K. Yoon, C.W. Park, H.Y. Ahn, D.H. Kim, Y.S. Lee and J. Kim, *J. Phys. Chem. Solids*, **68**, 780 (2007); https://doi.org/10.1016/j.jpcs.2007.03.028.
16. K. Suryakala, G.P. Kalaignan and T. Vasudevan, *Int. J. Electrochem. Sci.*, **1**, 372 (2006).
17. C.M. Julien and M. Massot, *Mater. Sci. Eng.*, **97**, 217 (2003); https://doi.org/10.1016/S0921-5107(02)00582-2.
18. D.K. Kim, P. Muralidharan, H.-W. Lee, R. Ruffo, Y. Yang, C.K. Chan, H. Peng, R.A. Huggins and Y. Cui, *Nano Lett.*, **8**, 3948 (2008); https://doi.org/10.1021/nl8024328.
19. D. Purwaningsih, R. Roto and H. Sutrisno, *Adv. Mater. Res.*, **1101**, 134 (2015); https://doi.org/10.4028/www.scientific.net/AMR.1101.134.
20. D. Purwaningsih, R. Roto and H. Sutrisno, *IOP Conf. Ser. Mater. Sci. Eng.*, **107**, 012033 (2016); https://doi.org/10.1088/1757-899X/107/1/012033.
21. D. Purwaningsih, R. Roto, Narsito and H. Sutrisno, *Adv. Mater. Res.*, **1123**, 100 (2015); https://doi.org/10.4028/www.scientific.net/AMR.1123.100.
22. S. Parvathy, R. Ranjusha, K. Sujith, K.R.V. Subramanian, N. Sivakumar, S.V. Nair and A. Balakrishnan, *J. Nanomater.*, **2012**, 1 (2012); https://doi.org/10.1155/2012/259684.
23. P. Bowen, *J. Dispersion Sci. Technol.*, **23**, 631 (2002); https://doi.org/10.1081/DIS-120015368.
24. A. Monshi, M.R. Foroughi and M.R. Monshi, *World J. Nano Sci. Eng.*, **2**, 154 (2012); https://doi.org/10.4236/wjnse.2012.23020.
25. X. Li, Y. Xu and C. Wang, *J. Alloys Comp.*, **479**, 310 (2009); https://doi.org/10.1016/j.jallcom.2008.12.081.
26. C.Y. Ouyang, S.Q. Shi and M.S. Lei, *J. Alloys Comp.*, **474**, 370 (2009); https://doi.org/10.1016/j.jallcom.2008.06.123.
27. P. Martín, M.L. López, C. Pico and M.L. Veiga, *Solid State Sci.*, **9**, 521 (2007); https://doi.org/10.1016/j.solidstatesciences.2007.03.023.